Growing actin networks form lamellipodium and lamellum by self-assembly
Supplemental material

Florian Huber, Josef Käs, and Björn Stuhrmann

This supplemental material contains a number of additional figures (Figs. 8 - 10) and moreover is devoted to further discuss three parts of the main article:

1 Filament Orientation

Several studies have revealed many salient features of the lamellipodial actin network architecture (1, 2). It has been discovered that the actin filaments in the networks are highly ordered, especially in the frontmost part of the cytoskeletal extension. Virtually all filaments are oriented with their fast growing plus ends towards the leading edge (1). The angular distributions display two characteristic peaks at $\pm 35^\circ$ with respect to the normal to the leading edge (2) that can be explained by Arp2/3 induced branch formation (3). To simplify our model, we mimicked the experimentally observed angular distribution taking two Gaussian distributions centered at $+35^\circ$ and -35°. The angular variance around the peak values was varied to study the effect on the simulation results (Fig. 1). As a consequence the appearance of the two dimensional actin network naturally changes, as can be seen in figure 1 A and in the pseudo fluorescence pictures (Fig. 2 B). However, changing the angular variance has almost no effect on the averaged one dimensional properties of the simulated actin network (Fig. 3). Therefore all data presented in the main article were obtained under the assumption that filaments take exactly $\pm 35^\circ$ angles with respect to the normal to the leading edge.

2 Nucleation

As mentioned in the appendix, we essentially tested two different nucleation models. The data shown in the main article were obtained under the assumption of a constant nucleation rate. This is a reasonable first approximation if Arp2/3 activation is considered the rate limiting step (4). In addition,

we did all parameter studies presented with a g-actin concentration dependent nucleation model. As a first estimate we assumed a linear dependence $r_{nuc} = N_0 \times G(0)$ between nucleation rate r_{nuc} and g-actin concentration at the leading edge $G(0)$. This leads to an uncapped plus end density for the steady state:

$$B = \frac{N_0 \times G(0)}{r_{cap}}. \quad (1)$$

Typical experimental values for $G(0)$ are $\sim$ 15 μM (5, 6). For the plus end density we expect $B \sim 100$ uncapped plus ends per micrometer of leading edge (7). Assuming that capping takes place with a rate of $r_{cap} \sim 1\ s^{-1}$ (8, 9), we estimate the nucleation rate constant to be $N_0 \sim 6\ \mu M^{-1}\mu m^{-1}s^{-1}$. The time evolution of the actin networks naturally differs between both nucleation models. Starting from purely monomeric actin the g-actin dependent nucleation model initially shows very high nucleation rates, unlike the constant nucleation model (data not shown). Upon variation of parameters such as r_{ac}, r_{tm}, r_{sev}, r_{anneal}, the system with g-actin dependent nucleation rate reacts slightly differently as well. However, qualitatively the behavior is the same as with constant nucleation. G-actin dependent nucleation acts as a feedback loop. We found that the g-actin dependent nucleation rate self-adjusted in such a way that the drop of velocity upon increased tropomyosin concentration, as well as the velocity increase upon increased ADF/cofilin concentration, were damped (Fig. 4). This also influences the depolymerization flux profiles. We present two graphs in this supplemental material that directly correspond to graphs from the main article but which have been obtained with the g-actin dependent nucleation model (parameters from table 1 and the main article, table 1). Figure 5 shows the simulation results in comparison to data from Svitkina et al. (1), demonstrating that both nucleation models are able to reproduce the fluorescence data (compare to main article, figure 4 A). Figure 6 presents the mean filament length curves for different severing and annealing rates and corresponds to figure 9 B,D in the main article.

In the future we intend to test numerous different nucleation models. Most of them include a strong f-actin dependence (10, 11). Very recently, an interesting 'monomer gating'model has been proposed that assumes a strong dependence of the concentration of capping protein and Arp2/3 (12).

3 Filament Severing

In order to understand the somewhat unexpected lengthening effect of filament severing, we complement our simulation results with an analytical

description. As described in the appendix we focus on one single, capped filament. Before severing, its length has the value of the mean filament length $\bar{l_0}$ (in μm). Assuming the filament gets fragmented at $t = 0$ we obtain two filaments, one of which has an uncapped plus end. Thus, the mean filament length drops to $\bar{l_0}/2$. Capping takes place with a rate $r_{cap} = 1\ s^{-1}$ (see text) such that the probability that the initially uncapped filament is still uncapped at time t is $exp(-r_{cap}\ t)$. Assuming a constant growth rate of $r_{on} \sim\ k_{on}\ G$ we get the mean plus end elongation (in μm) of the uncapped filament:

$$\Delta l^+(t) = \int_0^t (exp(-r_{cap}\ T) \times \delta\ r_{on})\, dT \tag{2}$$

$$= \frac{\delta\ r_{on}}{r_{cap}} \left[1 - exp(-r_{cap}\ t)\right]. \tag{3}$$

In addition, we assume that both filaments depolymerize at their minus end with approximately the same mean depolymerization rate r^-_{off}. The mean length of the uncapped filament (l_{uc}) along t is thus

$$\overline{l_{uc}}(t) = \overline{l_0}/2 + \Delta l^+(t) - \delta\ r^-_{off}\ t, \tag{4}$$

whereas the mean length of the capped filament develops with

$$\overline{l_c}(t) = \overline{l_0}/2 - \delta\ r^-_{off}\ t. \tag{5}$$

As a first approximation we assume a constant severing probability along the original filament of length $\overline{l_0}$. Thus, the capped filament fragment initially has lengths between 0 and $\overline{l_0}$, with equal probabilities for each. Due to the fact that this capped fragment vanishes when its length drops to zero, the resulting addition of $\overline{l_{uc}}$ and $\overline{l_c}$ has to be weighted by

$$\varphi(t) = \begin{cases} 0.5 + 0.5 \times \frac{r^-_{off}\ t}{\bar{l_0}/\delta}, & 0\ s \leq t < \frac{\bar{l_0}/\delta}{r^-_{off}}, \\ 1, & t \geq \frac{\overline{l_0}/\delta}{r^-_{off}} \end{cases} \tag{6}$$

thus leading to the total mean filament length $\bar{l}(t)$

$$\bar{l}(t) = \varphi(t) \times \overline{l_{uc}}(t) + (1 - \varphi(t)) \times \overline{l_c}(t) \tag{7}$$

$$= \overline{l_0}/2 - \delta\ r^-_{off}\ t + \varphi(t) \times \Delta l^+(t). \tag{8}$$

We also assume that the initial filament has a typical length of $\overline{l_0} \sim 0.5\ \mu m$, and that the g-actin concentration further back is $\sim 50\ \mu M$ (see main article, figure 1 D). Under these assumptions it turns out that filament severing

Symbol	Value	Description	Source
A	250 μM	Total actin concentration	(13, 14)
N_0	6 $\mu M^{-1}\mu m^{-1}s^{-1}$	Nucleation rate constant	see text

Table 1: Parameters and constants incorporated in the g-actin dependent nucleation model. All other parameters remain as described in the article (see article, table 1).

has a shortening effect only on very short time scales (Fig. 7). Taking typical filament life-times ($\sim$ 10 s to 1 min) we expect the overall effect of severing to be an increase of the mean filament length. However, to obtain an overall filament lengthening effect the g-actin concentration has to be above a certain threshold such that the growth of the uncapped fragment overcompensates the severing induced shortening. Depending on the parameters used this threshold is typically at $10 - 20$ μM (Fig. 7).

We found that the g-actin concentration increases nearly linearly from the front to the back (see article, Fig. 1 D). As illustrated in the article we observe two different regimes: in the front part the g-actin concentration is apparently too low to obtain an overall filament lengthening effect upon severing, while for $x \sim 2.5$ μm we clearly detect an increased mean filament length (see article, Fig. 9 B). The corresponding g-actin concentration at $x \sim 2.5$ μm was found to be $\sim$ 50 μM (main article, Fig. 1 D). Our method does not account for a realistic filament length distribution and we have not considered filament transport during the process. Thus, due to simplifications our analytical approach underestimates the threshold g-actin concentration for lengthening but nevertheless is able to qualitatively explain the findings from our simulation.

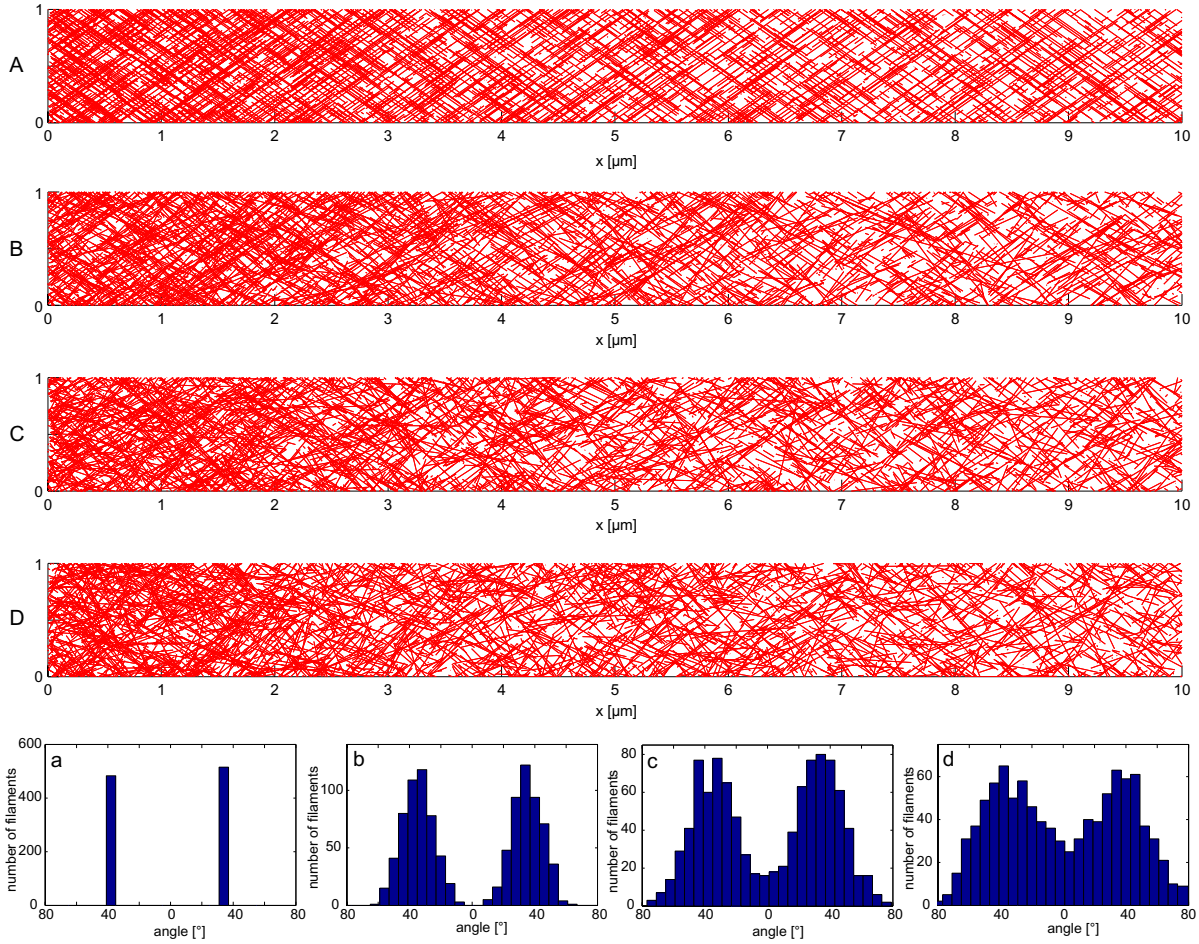

Figure 1: Simulated actin networks for different angular variances. (A-D) Simulated actin networks using parameters from the main article, table 1. (a-d) Distributions of all filament angles from the respective simulated networks A-D. (A,a) $Var(\phi) = 0°$, (B,b) $Var(\phi) = 10°$, (C,c) $Var(\phi) = 15°$, (D,d) $Var(\phi) = 20°$

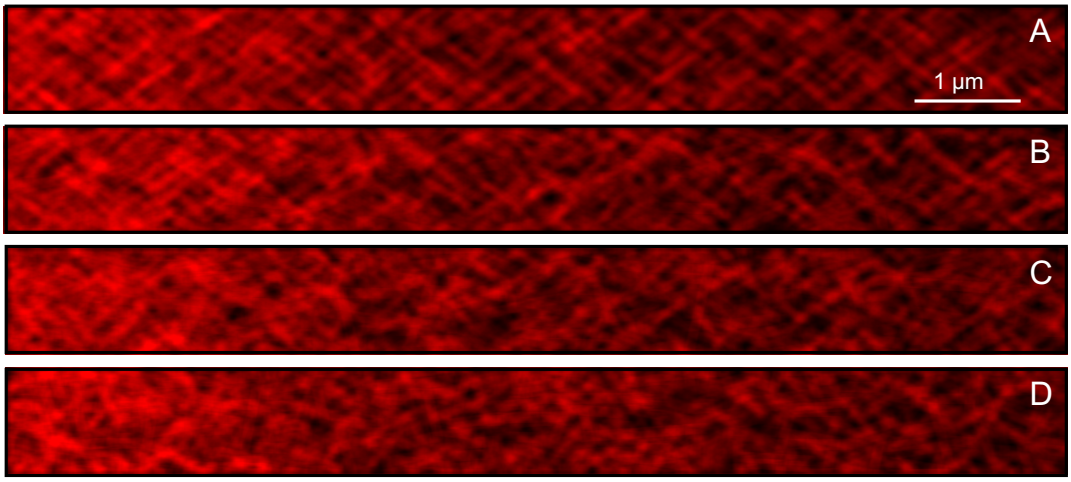

Figure 2: Pseudo fluorescence pictures of simulated actin networks for different angular variances. (A) $Var(\phi) = 0°$, (B) $Var(\phi) = 10°$, (C) $Var(\phi) = 15°$, (D) $Var(\phi) = 20°$. Respective simulated networks are shown in figure 1 A-D. Method adapted from (2)

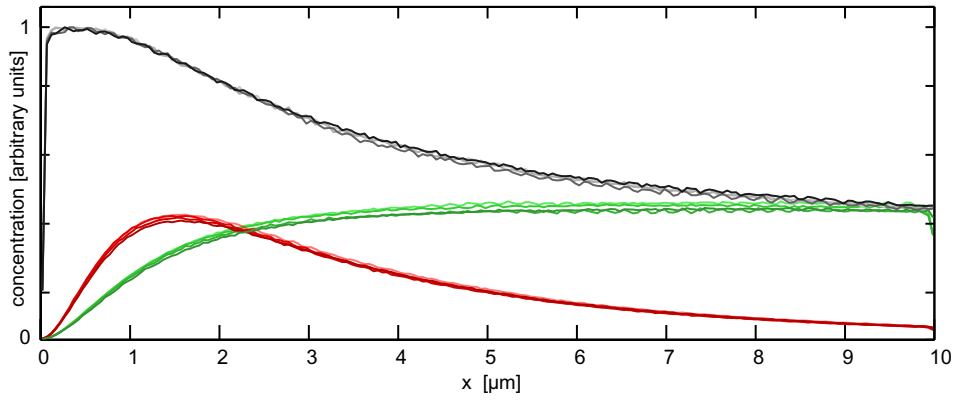

Figure 3: Normalized concentration curves for f-actin (grey), ADF/cofilin-f-actin (red) and tropomyosin-f-actin (green) for different angular variances $Var(\phi) = 0°$, $10°$, $15°$, $20°$. Differences clearly remain within the typical fluctuations

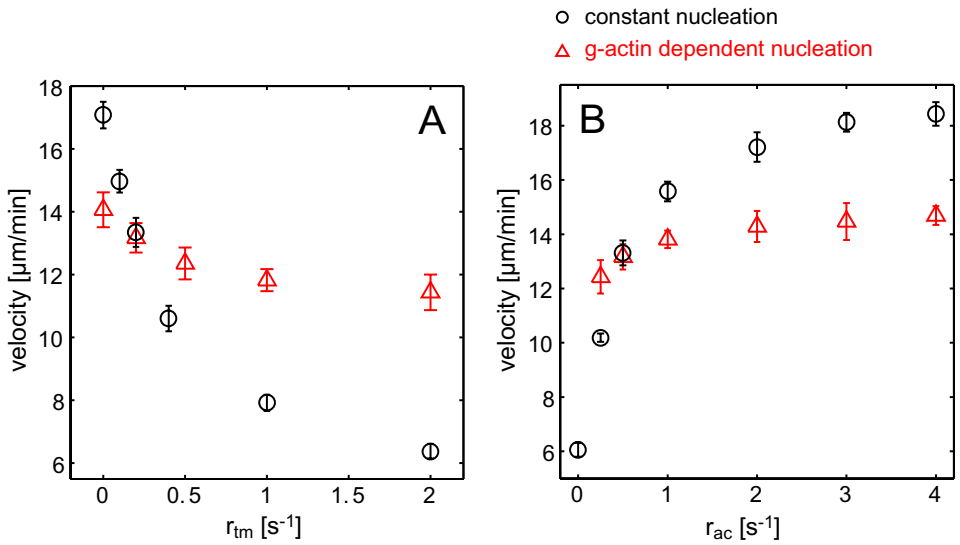

Figure 4: Comparison of g-actin dependent nucleation and constant nucleation model: Network growth velocities as functions of ADF/cofilin and tropomyosin binding rates. (A) Increased tropomyosin binding rates slow down network growth by limiting actin turnover. (B) Higher ADF/cofilin binding rates result in faster actin turnover, increasing network growth velocity. (A, B) Without the g-actin feedback mechanism the system reacts much more sensitively to variations of ADF/cofilin or tropomyosin. Error bars are standard deviations ($n = 8$ simulation runs for each data point)

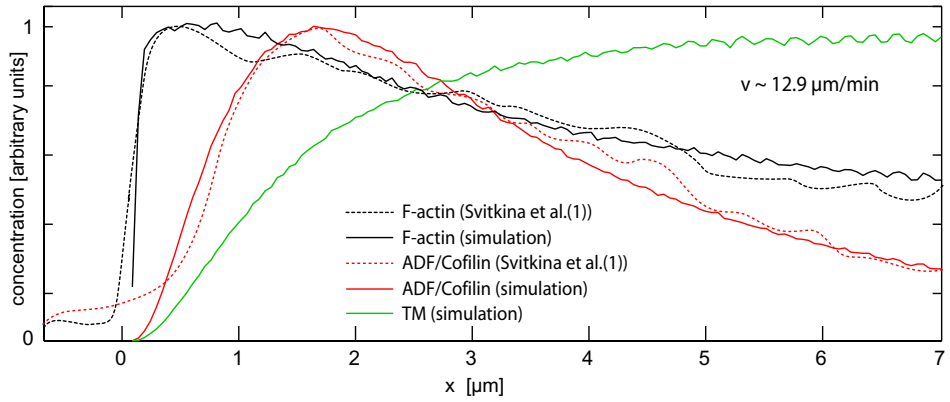

Figure 5: Simulated concentration curves for f-actin, ADF/cofilin-f-actin and tropomyosin-f-actin, normalized to compare results with experimental fluorescence curves (15) under the assumption of g-actin dependent nucleation. F-actin as well as ADF/cofilin-f-actin signals are in good agreement with data from Svitkina and Borisy (15). ADF/cofilin decorated f-actin dominates within the first $2-3\ \mu m$, whereas for $x \geq 2\mu m$, tropomyosin is the dominating element. AC: ADF/cofilin, TM: tropomyosin. The simulated data is nearly identical to that obtained with a constant nucleation rate (see main paper, Fig. 4 A)

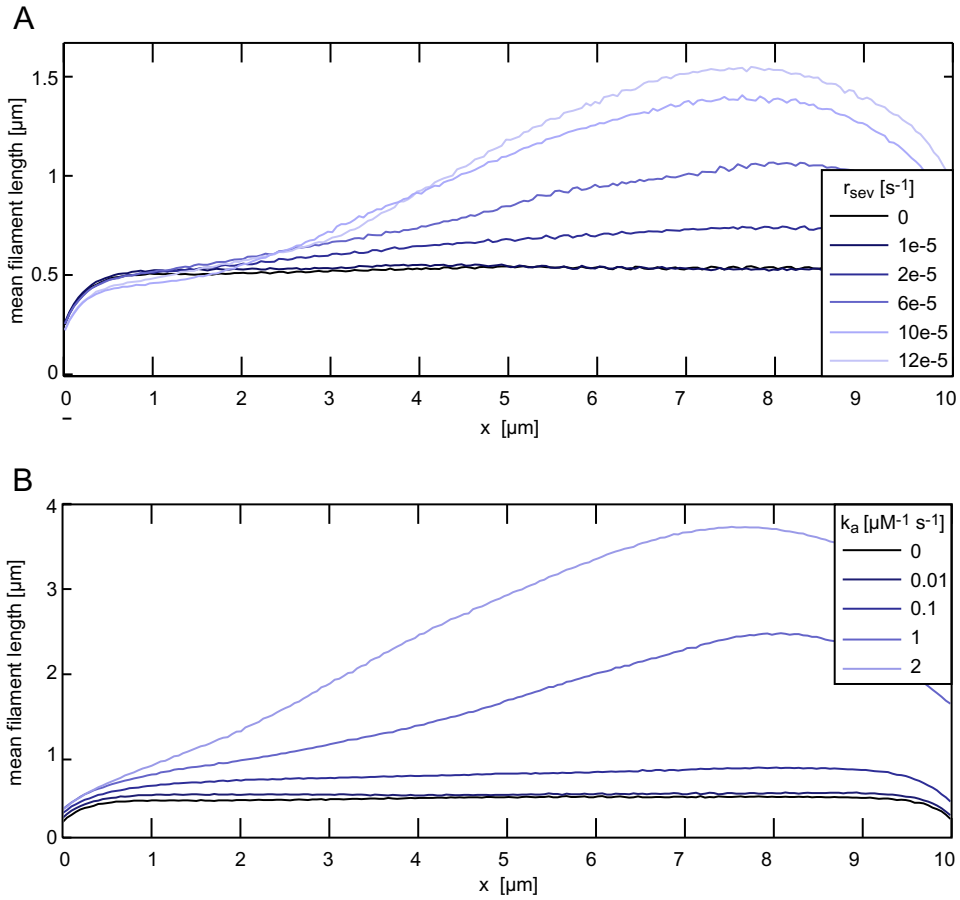

Figure 6: Filament severing (A) and annealing (B) significantly alter actin network design. G-actin dependent nucleation is assumed. Network behavior displays the same qualitative features as that obtained using a constant nucleation assumption (main article, Fig. 9 B,D). (A) Severing causes significantly increased mean filament lengths due to rapid elongation of newly created plus ends at the rear of the network filaments. (B) Mean filament length strongly increases upon enhanced annealing. This figure corresponds to figure 9 (B,D) from the main article

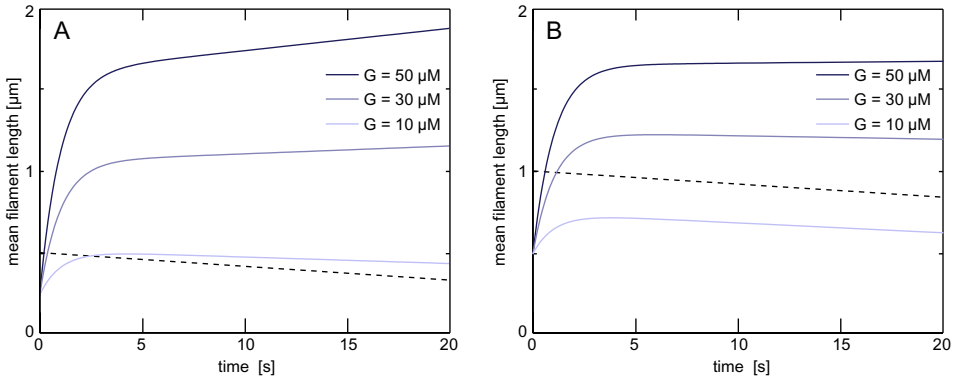

Figure 7: Mean filament length over time, following equation 8. Calculations were done with an initial length of $l_0 = 0.5\ \mu m$ (A) and $l_0 = 1\ \mu m$ (B), a mean minus end off rate of $r^-_{off} = 3\ s^{-1}$, and three different g-actin concentrations. The dashed line represents an unsevered filament of initial length $l_0 = 0.5\ \mu m$ (A) and $l_0 = 1\ \mu m$ (B). Above a certain threshold of g-actin concentration severing has a shortening effect on short time scales ($\sim$ few second) only, while on longer time scales the mean filament length increases. For all curves shown holds $t < \frac{\bar{l_0}/\delta}{r^-_{off}}$

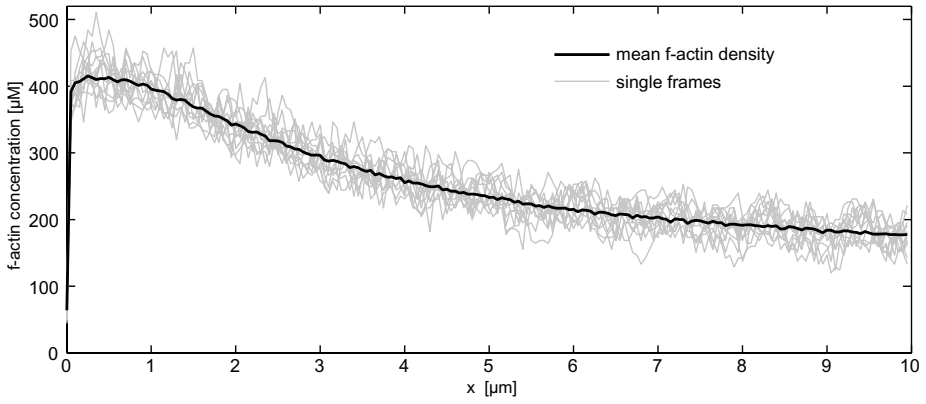

Figure 8: Smoothening of f-actin concentration distributions by averaging. The f-actin concentration curve (black) is the arithmetic mean of 60 frames, taken at intervals of 1 s of simulated time. For the sake of clarity only every fifth single frame curve is shown (gray)

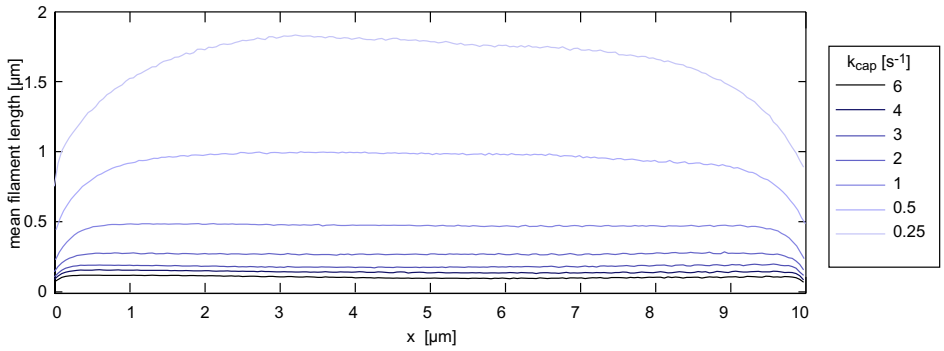

Figure 9: Mean filament lengths strongly depend on the capping rate. The capping rate, r_{cap}, was varied while adjusting the nucleation rate to keep the number of growing filaments constant.

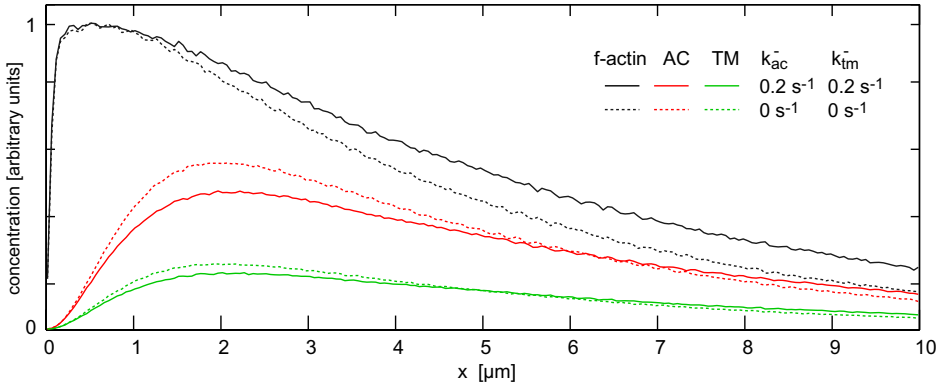

Figure 10: Absence of spatial separation of f-actin bound ADF/cofilin and tropomyosin in the case of equal actin unbinding rates for both actin-binding proteins. Results are shown for two different unbinding rates each. All concentrations are normalized with respect to the maximum f-actin concentration. All other rates were set to the values given in the main article, table 1

References

1. Svitkina, T. M., A. B. Verkhovsky, K. M. McQuade, and G. G. Borisy, 1997. Analysis of the Actin-Myosin II System in Fish Epidermal Keratocytes: Mechanism of Cell Body Translocation. *Journal of Cell Biology* 139:397–415.

2. Schaub, S., J.-J. Meister, and A. B. Verkhovsky, 2007. Analysis of actin filament network organization in lamellipodia by comparing experimental and simulated images. *Journal of Cell Science* 120:1491–1500.

3. Mullins, R. D., J. A. Heuser, and T. D. Pollard, 1998. The interaction of Arp2/3 complex with actin: Nucleation, high affinity pointed end capping, and formation of branching networks of filaments. *Proc Natl Acad Sci USA* 95:6181–6186.

4. Carlsson, A. E., 2003. Growth Velocities of Branched Actin Networks. *Biophysical Journal* 84:2907–2918.

5. Zigmond, S. H., 1993. Recent Quantitative Studies of Actin Filament Turnover During Cell Locomotion. *Cell Motility and the Cytoskeleton* 25:309–316.

6. Abraham, V. C., V. Krishnanmurthi, D. L. Taylor, and F. Lanni, 1999. The Actin-Based Nanomachine at the Leading Edge of Migrating Cells. *Biophysical Journal* 77:1721–1732.

7. Prass, M., K. Jacobson, A. Mogilner, and M. Rademacher, 2006. Direct measurement of the lamellipodial protrusive force in a migrating cell. *Journal of Cell Biology* 174:767–772.

8. Pollard, T. D., L. Blanchoin, and R. D. Mullins, 2000. Molecular Mechanisms Controlling Actin Filament Dynamics in Nonmuscle Cells. *Annu. Rev. Biophys. Biomol. Struct.* 29:545–576.

9. Schafer, D. A., P. B. Jennings, and J. A. Cooper, 1996. Dynamics of Capping Protein and Actin Assembly In Vitro: Uncapping Barbed Ends by Polyphosphoinositides. *Journal of Cell Biology* 135:169–179.

10. Beltzner, C. C., and T. D. Pollard, 2008. Pathway of Actin Filament Branch Formation by Arp2/3 Complex. *Journal of Biological Chemistry* 283:7135–7144.

11. Dawes, A. T., G. B. Ermentrout, E. N. Cytrynbaum, and L. Edelstein-Keshet, 2006. Actin filament branching and protrusion velocity in a simple 1D model of a motile cell. *Journal of Theoretical Biology* 242:265–279.

12. Akin, O., and R. D. Mullins, 2008. Capping Protein Increases the Rate of Actin-Based Motility by Promoting Filament Nucleation by the Arp2/3 Complex. *Cell* 133:841–851.

13. Mogilner, A., and L. Edelstein-Keshet, 2002. Regulation of Actin Dynamics in Rapidly Moving Cells: A Quantitative Analysis. *Biophysical Journal* 83:1237–1258.

14. Fleischer, F., R. Ananthakrishnan, S. Eckel, H. Schmidt, J. Käs, T. Svitkina, V. Schmidt, and M. Beil, 2007. Actin network architecture and elasticity in lamellipodia of melanoma cells. *New Journal of Physics* 9:420.

15. Svitkina, T. M., and G. G. Borisy, 1999. Arp2/3 Complex and Actin Depolymerization Factor/Cofilin in Dendritic Organization and Treadmilling of Actin Filament Array in Lamellipodia. *Journal of Cell Biology* 145:1009–1026.